

Originally published as:

Dimitriadis, I., Papazachos, C., Panagiotopoulos, D., Hatzidimitriou, P., Bohnhoff, M., Rische, M., Meier, T. (2010): P and S velocity structures of the Santorini-Coloumbo volcanic system (Aegean Sea, Greece) obtained by non-linear inversion of travel times and its tectonic implications. - Journal of Volcanology and Geothermal Research, 195, 1, 13-30

DOI: 10.1016/j.jvolgeores.2010.05.013

# ***P* and *S* velocity structure of the Santorini – Coloumbo volcanic system (Aegean Sea, Greece) obtained by non-linear inversion of travel times and its tectonic implications**

I. Dimitriadis<sup>1,\*</sup>, C. Papazachos<sup>1</sup>, D. Panagiotopoulos<sup>1</sup>, P. Hatzidimitriou<sup>1</sup>, M. Bohnhoff<sup>2</sup>, M. Rische<sup>3</sup> and T. Meier<sup>3</sup>

<sup>1</sup>*Geophysical Laboratory, Department of Geology, Aristotle University of Thessaloniki, GR-54124 Thessaloniki, Greece*

<sup>2</sup>*GeoForschungsZentrum, Telegrafenberg D424, 14473 Potsdam, Germany*

<sup>3</sup>*Department of Geosciences, Ruhr-University Bochum, Germany*

## **Abstract**

One of the most prominent tectonic features of the Eastern Mediterranean region is the Hellenic volcanic arc in the Southern Aegean Sea, with the Santorini Island being its most active volcanic center. Recent seismic studies show that the main seismic activity of the Santorini volcanic center is strongly associated with the volcanic processes, as well as with the seismo-tectonic regime of the broader Southern Aegean Sea area. The main cluster of local seismicity is located near the north-eastern edge of the Santorini Island, beneath the Coloumbo Reef, which is a submarine volcanic seamount of the Santorini Island volcanic system.

The *P* and *S* wave velocity structure of the Santorini – Coloumbo volcanic system is studied by inverting travel-times of local earthquakes recorded by two independent dense seismic arrays installed in the broader area of Santorini islands during the period September 2002 – September 2005. In particular, 137 local earthquakes with 1600 *P*-phases and 1521 *S*-phases recorded by 25 seismological stations have been selected for the inversion. The inversion technique applied is non-linear, since three-dimensional ray tracing is incorporated. The reliability of the final tomographic results is demonstrated through resolutions tests using synthetic seismic data.

The obtained results confirm the strong variations of the *P* and *S* wave velocity structure in the area of Santorini – Coloumbo volcanic system, as well as the

\* Corresponding Author. Tel.: +30-2310998535 Fax: +30-2310998528

E-mail address: [iordanis@geo.auth.gr](mailto:iordanis@geo.auth.gr) (I.M. Dimitriadis)

connection between the tectonic setting of the study area with the magmatic processes taking place beneath the two volcanoes. The tomographic models show that a low-velocity zone extends along the north-eastern edge of the Santorini Island, parallel to the “Kameni – Coloumbo” fracture zone (NE – SW direction), which corresponds to the western termination of the major ENE – WSW Santorini – Amorgos Fault Zone. Evidence is presented that this structural lineament corresponds to a tecto-volcanic fracture zone, which probably links the volcanic center of Santorini with the submarine volcano at Coloumbo Reef. Furthermore, the tomographic results show that the magmatic chamber beneath the Coloumbo volcanic seamount is probably located at depth of 6-7 km in good agreement with recent independent studies in the area.

**Keywords:** Santorini volcanic center; Aegean Sea; Seismic tomography; Non-linear inversion; 3-d velocity structure; Low-velocity zone.

---

## 1. Introduction

The volcanic center of Santorini Island is one of the most active volcanoes of the southern Aegean volcanic arc. The volcanic arc is a major geo-tectonic feature of the Aegean Sea subduction system, resulting from the convergence between the African oceanic lithosphere and the Eurasian continental lithosphere. In particular, the northern part of the eastern Mediterranean plate subducts under the overriding Aegean micro-plate, at an approximately rate of 3.5 – 4.0 cm/a, leading to the formation of an inclined Benioff seismic zone up to the depth of about 150 – 200 km (Papazachos and Comninakis, 1971; McKenzie, 1972; McClusky et al., 2000; Meier et al., 2004; Papazachos et al., 2000; Papazachos et al., 2005).

Recent seismic studies in the broader area of Santorini volcanic center show that the main seismic activity of this area is strongly associated with the tectonic regime, as well as with the volcanic processes (e.g., Bohnhoff et al., 2004, 2006; Dimitriadis et al., 2005, 2009; Hensch et al., 2008). In particular, the local seismicity is mainly located near the north-eastern edge of the Santorini Island, at the Coloumbo seamount, a submarine volcano that has a well defined 1500-meter-wide crater, a crater rim as shallow as 17 meters and a crater floor ~500 meters below the sea level

(Perissoratis, 1995; Francalanci et al., 2005; Sigurdsson et al., 2006). In contrast, the main caldera of the Santorini volcano is characterized by the almost complete absence of seismicity (Dimitriadis et al., 2005, 2009; Bohnhoff et al., 2006; Hensch et al., 2008). Furthermore, these studies concluded that the seismic activity in the broader area of Santorini – Coloumbo volcanic system follows an ENE – WSW direction along the Santorini – Amorgos Ridge. The intense activity at Coloumbo area is in good agreement with the recent marine surveys that show an intense hydrothermal activity with fluid temperatures greater than 200°, in comparison to the corresponding low-level activity of the Santorini caldera (fluid temperatures ~ 15-20°) (Sigurdsson et al., 2006).

Neotectonic and structural field observations show that the Coloumbo area and the northern Santorini volcanic center is dominated by a NNW – SSE extensional stress regime that produces a major fault zone of NE – SW strike (approximately 35° – 40°). This zone is called “Kameni – Coloumbo” fracture zone (Fytikas et al., 1990; Vougioukalakis et al., 1995; Mountrakis et al., 1996) and coincides with the alignment of the volcanic centers. In particular, several fault sites have been studied in the north-eastern edge of Thera Island at Cape Coloumbo area, which exhibit intense strike-slip and normal faulting in a NE – SW trending zone. A major dextral strike-slip fault zone of NE – SW strike (approximately 35° – 40°) confines the deformation zone to the southwest, while smaller normal faults of NE – SW strike (approximately 40° – 70°) belong to the same zone. In addition, the dykes present along the caldera walls in the north-eastern part of the caldera follow the same alignment of NE – SW direction, in agreement with a dominant extension of NW – SE direction (Fytikas et al., 1990; Mountrakis et al., 1996).

Focal mechanisms and stress tensor inversion results (Dimitriadis et al., 2009) show that the cluster of the earthquakes at the Coloumbo volcano is strongly associated with the “Kameni – Coloumbo” fracture zone (NE – SW direction), which corresponds to the western termination of the major ENE-WSW Santorini – Amorgos Fault Zone. Moreover, a ~20-30° rotation of the local stress field was observed with respect to the NNW-SSE regional extension field of the southern Aegean Sea.

In the present study travel times of local earthquakes recorded by two temporary networks installed in the broader area of Santorini Islands are used to determine the 3-d *P* and *S* velocity structure of the Santorini – Coloumbo volcanic system. The results are interpreted with respect to the geological structure, the local tectonic setting and

the magmatic processes of the area under study, which is the most active volcanic system in the Eastern Mediterranean region.

## **2. Travel time data**

The data used in the present work are the  $P$  and  $S$  arrival times from local earthquakes recorded by two independent dense seismic arrays installed in the broader area of Santorini islands during the period September 2002 – September 2005.

The first seismic array used was a local network consisting of fourteen (14) seismological stations, equipped with three-component broadband seismometers, which was deployed on the Santorini islands. Ten stations have been installed on the main island (Thera Island), two stations on the smaller island of Thirasia and two stations on the newly formed intra-calderic islands of Palaea and Nea Kameni (open triangles in Figure 1). The average distance between the fourteen broadband stations was of the order of 3 km. This temporary seismic array was in operation between the end of March 2003 and the beginning of September 2003. During this time period, 159 best-located earthquakes were recorded in the broader area of Santorini – Coloumbo volcanic system (Dimitriadis et al., 2009).

The second seismic array used was the CYCNET temporary seismological network, which was a 22-station network installed in the broader Cyclades area between September 2002 and September 2005 (Bohnhoff et al., 2006). In order to discern the events recorded in the broader area of Santorini – Coloumbo volcanic system, we only used stations which were installed on the Santorini complex and on islands surrounding it. In particular, stations installed on west Amorgos Island (AMOW), on Anaphe Island (ANAF), on Ios Island (IOSI), on Anydros islet (ANID) and six stations installed on the Santorini islands (NEAK, SANC, SANN, SANS, SANT, THIR) were used (black squares in the Figure 1). Furthermore, recordings from a few OBS (Ocean Bottom Seismometers) stations installed in the Santorini – Amorgos area during the period January – March 2005 were also employed (black squares in the Figure 1). In total, 378 best-located earthquakes were recorded during the period September 2002 – September 2005 in the broader area of the Santorini – Coloumbo volcanic system.

In order to create a unique database of  $P$  and  $S$  arrival times, earthquakes recorded by both arrays were selected, resulting in an initial data set of 409 local earthquakes

with 3742 *P*-phases and 3528 *S*-phases recorded at 35 stations. In Figure (1) the distribution of the selected epicentres is presented. It is clear that the main cluster of the seismic activity is located near the north-eastern edge of the Santorini Island, at the Coloumbo seamount. Moreover, a very low seismicity level is observed under the main caldera of the Santorini volcanic center during the same time period. Furthermore, a small cluster of events near the Anydros islet is located in a direction almost along the main tectonic feature of the area under study, the Santorini – Amorgos Fault Zone (NE – SW direction) (Figure 1).

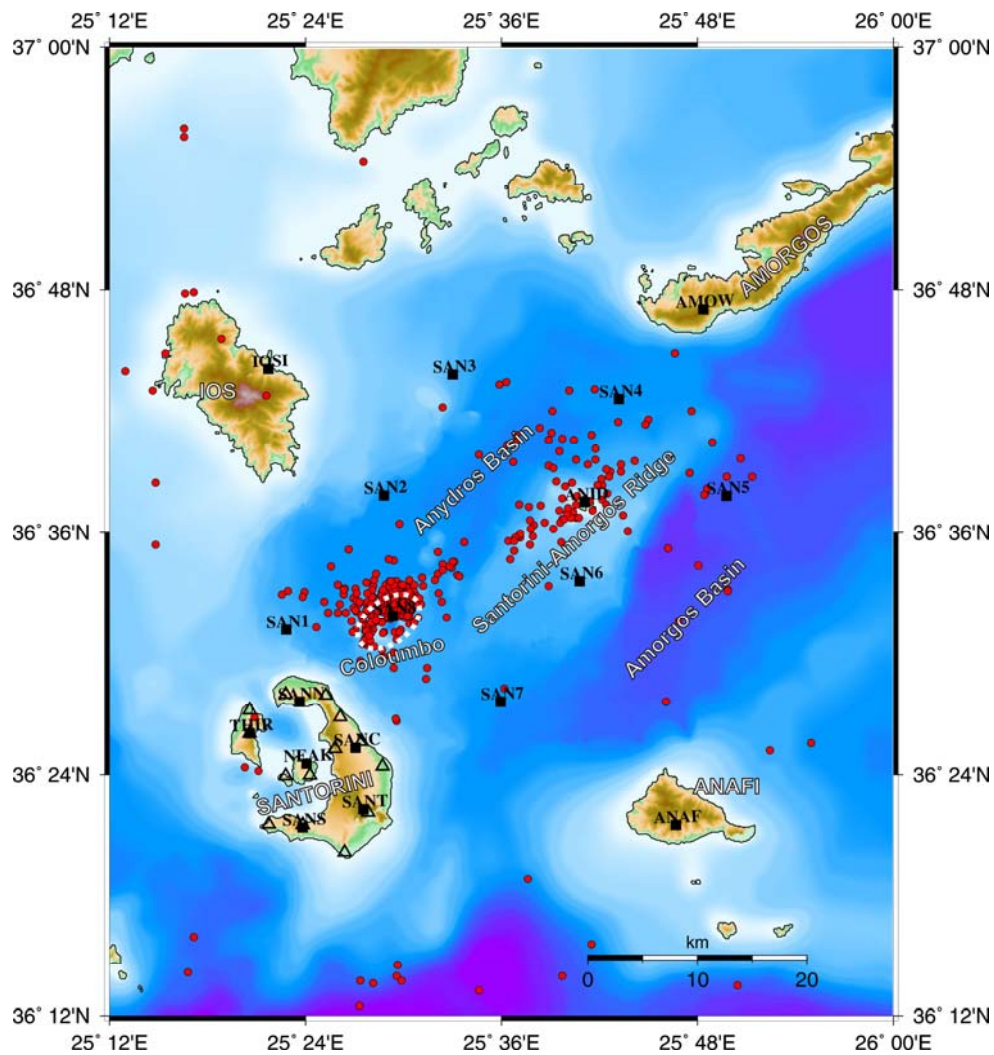


**Figure 1:** Epicenters of the 409 local best-located events recorded by two local arrays operating in the broader Santorini area between mid2002-mid2005. Open triangles correspond to temporary seismological stations installed on Santorini Islands, while the black squares denote the CYCNET stations from which data have been used (see text for details). The dashed ellipse denotes the position of the Coloumbo seamount.

In order to determine a 3-d  $P$  and  $S$  velocity structure of the Santorini – Coloumbo volcanic system, a sub-region has been selected ( $36.585$ - $36.320^{\circ}$ N and  $25.580$ - $25.315^{\circ}$ E) which includes the Santorini complex, along with the Coloumbo seamount, as is shown by the box in Figure (2). The final data set used for the tomographic inversion consists of 137 local earthquakes with 1600  $P$ -phases and 1521  $S$ -phases recorded at 25 seismological stations. Furthermore, the results from a double-difference relocation procedure were used, in order to have optimal initial focal parameters for these earthquakes. The relocation procedure is based using a modified version of the computer program HYPO-DD (Waldhauser, 2001) which employs the double-difference earthquake relocation algorithm (Waldhauser and Ellsworth, 2000; Waldhauser, 2001) and re-weights the residual double-difference threshold differently, depending on the type of phase used ( $P$  or  $S$ ) (Dimitriadis et al., 2009). The distribution of the epicenters of the relocated events is shown in Figure (2), along with the recording stations used in the inversion.

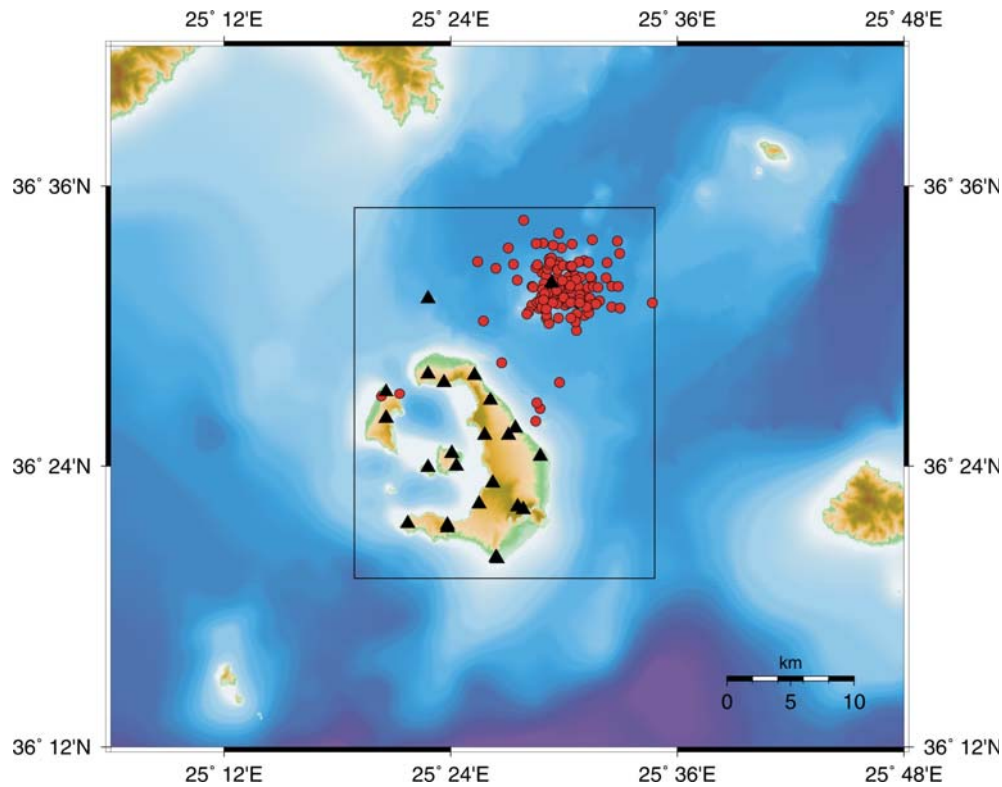


**Figure 2:** Epicenters of the 137 selected relocated local events used for tomography. The study area is denoted with the black box, while triangles denote the recording stations used.

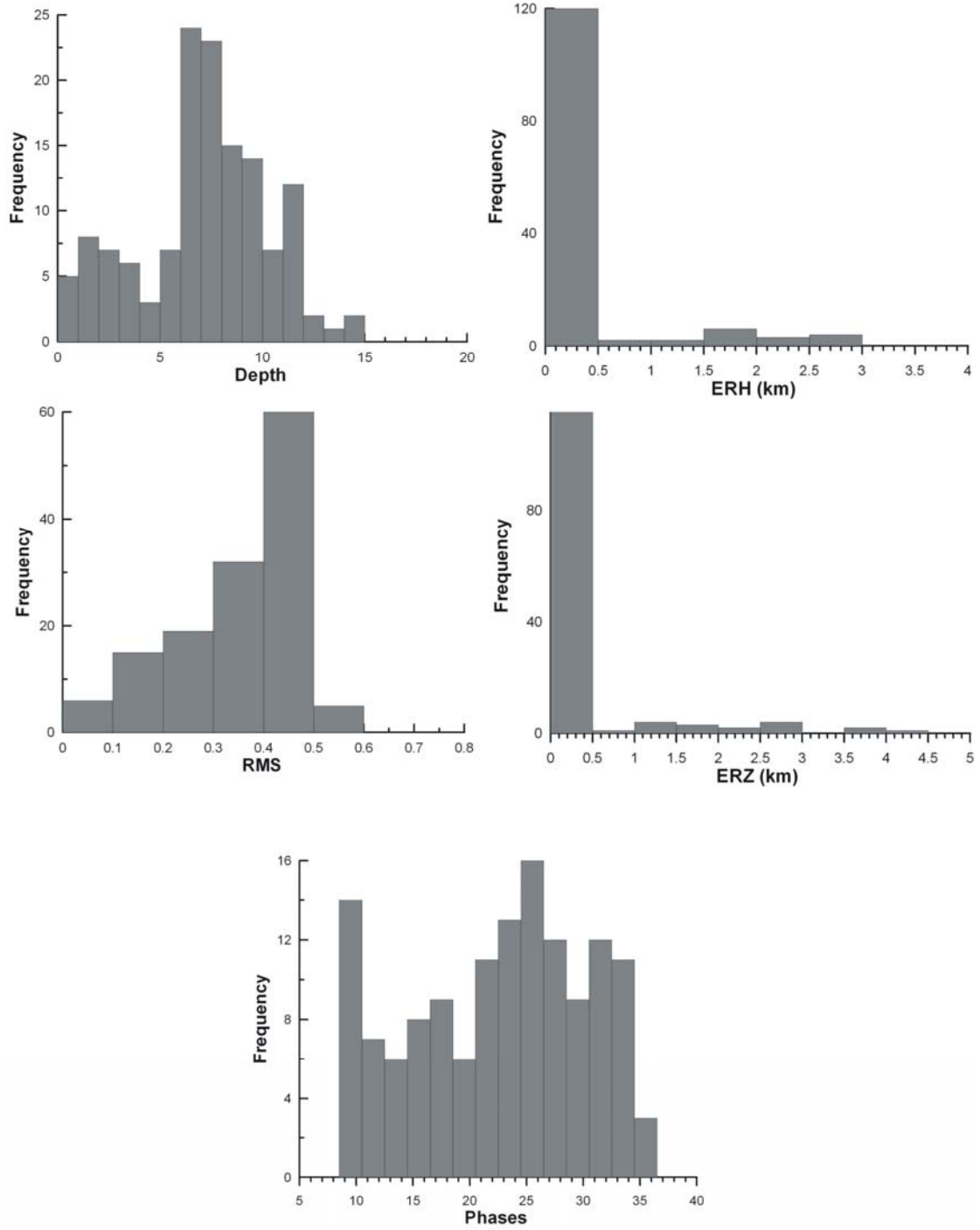


**Figure 3:** Histograms of the relocation parameters (focal depth, RMS, ERH, ERZ, number of P and S phases) for the 137 selected local events used in the inversion procedure.

The total length of seismic rays that sample the study area was approximately 50000 km. Most events are shallow with depths less than 10 km, RMS travel time error less than 0.5 s and hypocentral errors (ERH and ERZ) less than 0.5 km. Furthermore, most earthquakes employed in the tomographic procedure had more than 10 phases (see histograms in Figure 3).

### 3. Inversion procedure

The inversion procedure used in this study is based on the original method of travel-time inversion of local earthquakes, as proposed by Aki and Lee (1976). According to their approach, the travel-time residual can be expressed as a function of the perturbations of the earthquake's hypocentral parameters and slowness of the model. A linear system of equations is derived:

$$\mathbf{R} = \mathbf{H}\Delta\mathbf{h} + \mathbf{P}\Delta\mathbf{u} \quad (1)$$

where  $\mathbf{R}$  is the travel-time residuals vector,  $\mathbf{H}$  and  $\mathbf{P}$  are the hypocentral and slowness Jacobian (derivative) matrices, and,  $\Delta\mathbf{h}$  and  $\Delta\mathbf{u}$  are the hypocentral and slowness corrections vectors, respectively. It is possible to write equation (1) as a single linear system of the form:

$$\mathbf{R} = \mathbf{A}\mathbf{x} \quad (2)$$

The large number of the unknown parameters, along with the inversion instability does not allow obtaining a simple least-squares solution for this linear system. The typical approach is to consider additional constraints and minimize an appropriate model norm (e.g., Crosson, 1976; Thurber, 1983). In this study we used the approach proposed by Papazachos and Nolet (1997a, b) for the solution of this equation. According to this approach, equation (2) is modified as follows:

$$\mathbf{C}_d^{-1/2} \mathbf{A} \mathbf{C}_x^{1/2} \mathbf{z} = \mathbf{C}_d^{-1/2} \mathbf{d} \quad (3)$$

$$\lambda \mathbf{I} \mathbf{z} = 0 \quad (4)$$

where  $\mathbf{C}_d$  is the covariance matrix of the data,  $\mathbf{d}$ ,  $\mathbf{C}_x$  is the *a priori* estimate of the covariance matrix (usually diagonal) of the model,  $\mathbf{x}$ , and  $\lambda$  is a constant which regulates the strength of our additional minimum norm (damping) constraints.

In this approach, the final solution is given by the following equation:

$$\mathbf{x} = \mathbf{C}_x^{1/2} \mathbf{z} \quad (5)$$

where,  $\mathbf{C}_x^{1/2}$ , is a diagonal matrix which contains our preliminary estimate of the square root of the *a posteriori* model covariance matrix, in an attempt to reduce relative errors in the final solution (Papazachos and Nolet, 1997a).

For the model configuration, the earth is embedded in a rectangular grid of nodes and the slowness at each point is calculated by trilinear interpolation (Thurber, 1983). A grid consisting of 2431 *P* and *S* velocity nodes was defined, with a horizontal and vertical grid spacing set to 2 km. The specific grid size was selected to be slightly smaller than the typical size of the resolved anomalies, as is later presented. The Cartesian geometry simplifies all computations, especially those concerning the 3-d ray tracing, though a small number of nodes lies outside the earth.

A three-dimensional ray tracing technique was applied in this study, namely the revised bending algorithm proposed by Moser et al. (1992). In this approach, rays are represented by beta splines (generalized B-splines), which are defined by support points. A conjugate gradient method is used to optimize the distribution of these points in order to minimize the travel time. This method is fully three-dimensional and shadow areas (due to low-velocity zones) where diffracted arrivals may be first arrivals do not pose any problems to the algorithm (Wielandt, 1987; Papazachos and Nolet, 1997a).

The most important problem for ray bending is that if the starting ray is far from the global minimum, a secondary arrival may be determined. For this reason, the initial paths of the rays used have been derived from graph theory, using a modification proposed by Moser (1991). The graph theory methods systematically search in a network of nodes for the shortest path to a specific point. A significant limitation of this theory is that the accuracy of this method depends on the density of nodes and the angular discretization imposed by the grid (Moser, 1991; Papazachos and Nolet, 1997b).

## 4. Data processing

Several studies (e.g., Spakman, 1988; Kissling et al., 1994) have demonstrated the importance of the background 1-d model for tomographic purposes, especially in non-linear inversions where the geometry of rays in the initial 1-d model critically influences the final results. For the background 1-d model we used the local velocity

model proposed by Dimitriadis et al. (2009) for the area of Santorini – Coloumbo volcanic system, which has been determined by a 1-D inversion of local seismic phases, using a large number of starting models. Since the data set used for the determination of this model consists of earthquakes which mostly occurred at depths between 2 and 9 km, the corresponding velocity model has a relatively poor resolution for very shallow depths. Moreover, the near-vertical incidence of rays close to the surface limits the control of the shallow velocity structure. Hence, it is possible that the estimated  $P$ -velocities for the surface layers ( $\sim 0 - 2$  km) are biased (e.g. overestimated, Dimitriadis et al., 2009).

Since the additional model norm minimization usually employed in tomographic inversion is based on the assumption that the perturbations of the derived parameters (slowness, earthquake locations) follow a normal distribution, it is necessary to have *a priori* estimates of the variations of each parameter. On the basis of the accuracy of the hypocentral estimations of the area under study (see histograms in Figure 3), the values of 0.3 s for the origin time, 2 km for the horizontal and 4 km for the vertical direction were adopted for the *a priori* standard errors. For the slowness,  $S_P$  and  $S_S$  the values of 0.03 s/km and 0.05 s/km were used, respectively, based on the previously published tomographic results for the crust and uppermost mantle of the broader South Aegean Sea area (Papazachos and Nolet, 1997a).

Furthermore, several damping coefficients,  $\lambda$ , were tested with real and synthetic data (presented later) and the value of 2 was finally used, slightly larger than the theoretical value of 1 (Franklin, 1970), which is valid if our *a priori* estimates for the data and model covariance matrices are correct. However, since neither the model perturbations, nor the travel-time residual distribution is not completely Gaussian, the use of larger values is often necessary to stabilize inversion results, in order to ensure the robustness of the solution to travel-time outliers.

Due to the large number of unknowns, the final inversion (solution of equation 2) was solved with LSQR (Paige and Saunders, 1982). Since a non-linear approach was adopted, after each LSQR iteration matrix  $A$  was recomputed using the three-dimensional bending ray tracing algorithm and the new linear system was repeatedly solved until no significant misfit change was observed.

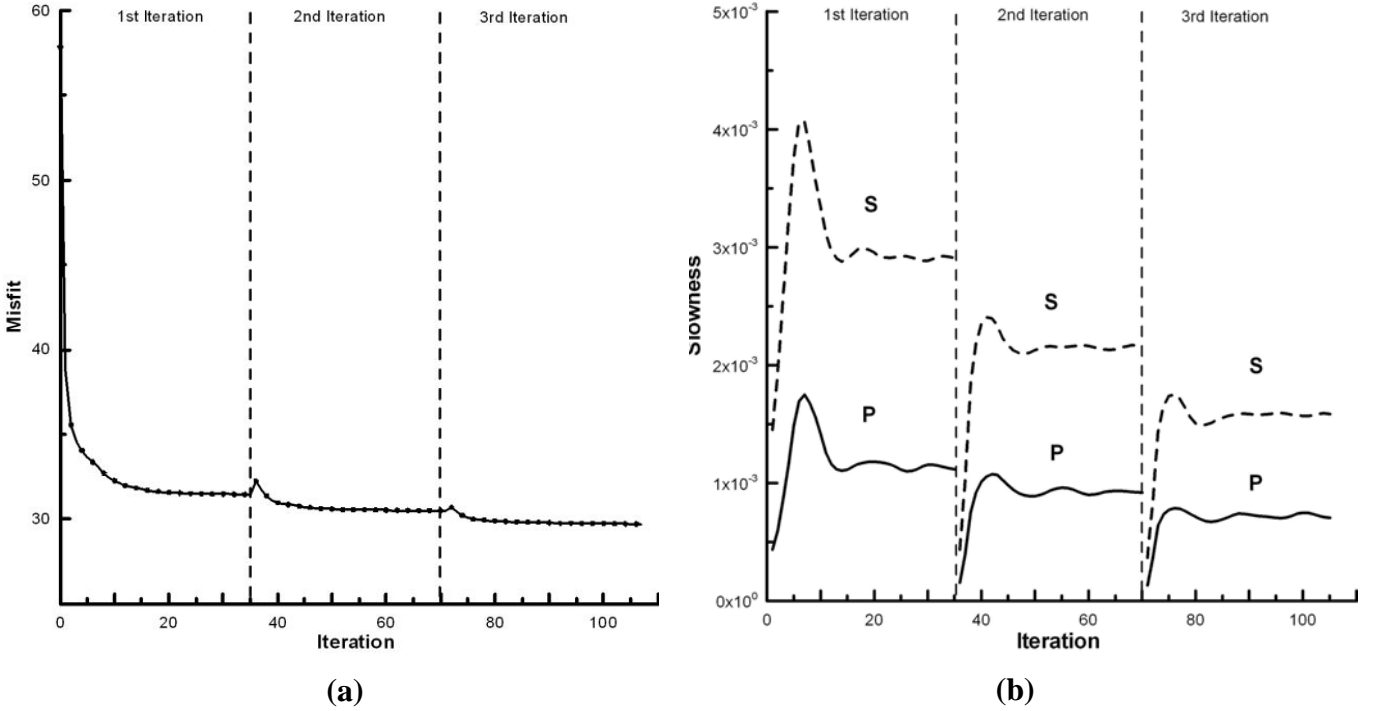


**Figure 4:** (a) Plot of the misfit reduction for the three non-linear iterations versus LSQR steps. Note the increase of the misfit (arbitrary units) between iterations. (b) Plot of the model ( $P$  and  $S$  slowness perturbation) norm for the three non-linear iterations versus LSQR steps.

The inversion was performed in 3 iterations. At each iteration, the maximum number of steps in LSQR (linear steps) was determined empirically ( $\sim 35$  steps), when both the misfit and the  $P$ - and  $S$ -velocity perturbation norms did not show significant variation. Figure (4a) shows the variation of the misfit for each LSQR step, while Figure (4b) shows the  $P$  and  $S$  slowness model norm for each iteration. Between two successive iterations a misfit increase is observed (Figure 4a), due to the non-linearity of the problem, in accordance with various tomographic studies and synthetic tests (e.g. Sambridge, 1990; Papazachos and Nolet, 1997b). This jump is simply the expected difference between linear (end of each iteration) and non-linear (start of next iteration) misfit estimation (Tarantola, 1987). This pattern suggests that LSQR should be stopped in advance from mathematical convergence, since most of the model anomaly has been retrieved and additional iterations usually lead to an increase of the true, non-linear data misfit (Papazachos and Nolet, 1997b).

## 5. Resolution tests

Before presenting the final results, the resolution of the obtained tomographic images needs to be evaluated. Since no direct information about the resolution and covariance of the final solutions can be obtained when using a conjugate gradient method such as LSQR, only tests with synthetic data can provide some insight on the solution quality. The advantage of such tests is that they provide an overall estimation of the effect of not only data quality but also model parameterization and damping on the solution quality (Kissling et al., 2001).

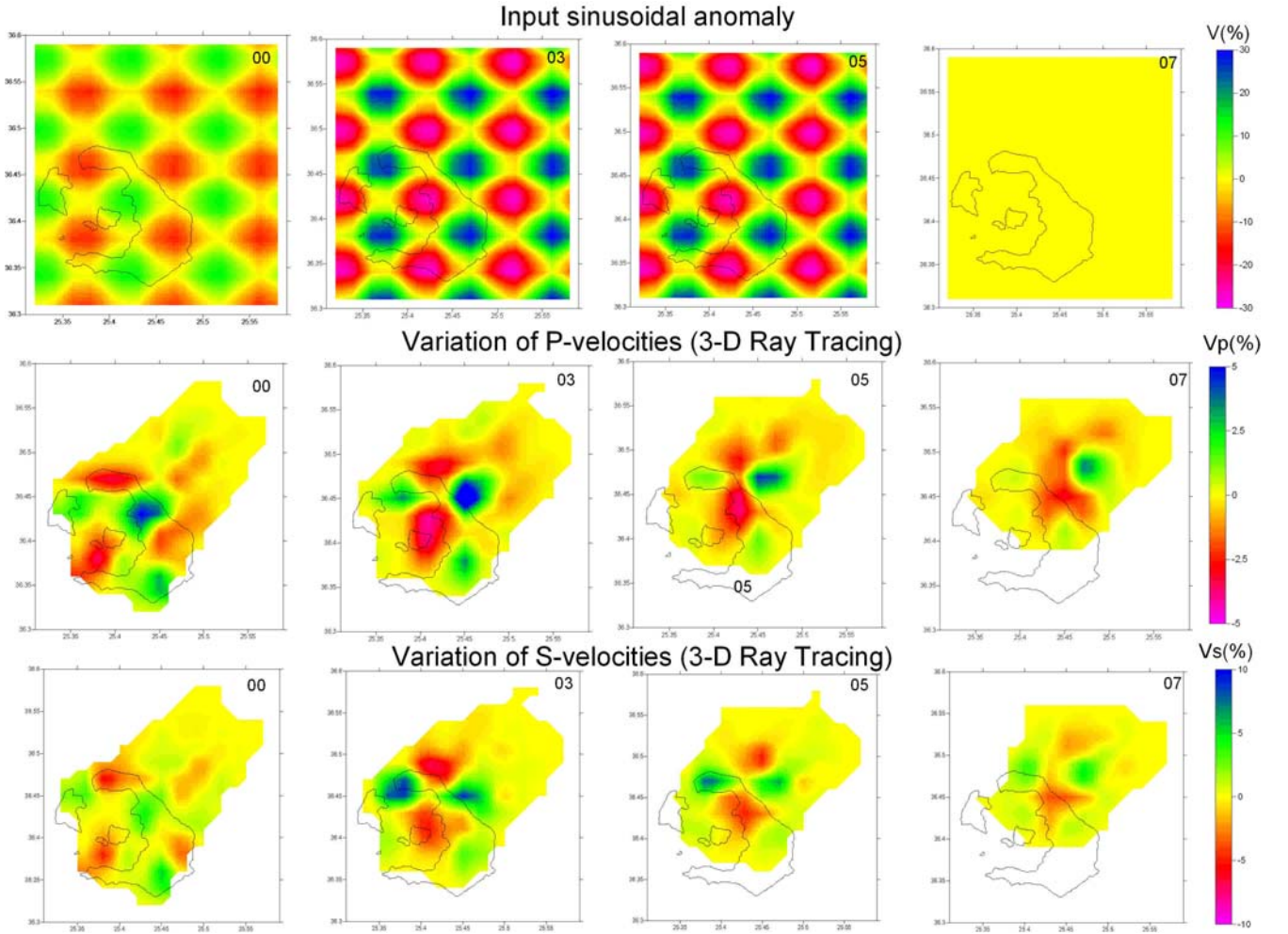


**Figure 5:** Checkerboard pattern tests for various depths (0 km, 3 km, 5 km and 7 km) for a sinusoidal input anomaly of 40% with wavelengths of 6 km (anomaly size ~3km) for both horizontal and vertical dimensions. In the middle and bottom figures the results of the resolution tests for  $P$  and  $S$  velocities are shown, respectively, using the 3-D ray non-linear inversion algorithm.

In the present study, we have chosen to perform “checkerboard” tests (Spakman, 1988; Humphreys and Clayton, 1988; Papazachos and Nolet, 1997a). In particular,

several “checkerboard” tests have been performed using a sinusoidal perturbation of 40% (which corresponds to a usual anomaly amplitude for a volcanic system area) of various wavelengths. The same wavelength has been used for both horizontal and vertical dimensions and for all tests random noise with a standard deviation proportional to the data quality has been added to the synthetic travel times (0.2 s for *P* waves and 0.3 s for *S* waves).

The results presented in Figures (5) and (6) correspond to input anomalies of 40%, with half-wavelengths (size of positive or negative perturbation area) of 3 km for both horizontal and vertical dimensions. As can be observed in the Figure (5), as the depth is increasing the resolution of the results becomes poorer. In practice, the resolution depth limit for our data set is of the order of 7 km. Moreover, anomalies in the area of the Coloumbo seamount are only partially recovered, especially for shallower depths (Figure 5).

Furthermore, two cross sections are presented in order to further evaluate the resolution of our data set (Figure 6). The first cross-section along line A has a NW – SE direction, while the second cross section (line B) is perpendicular to line A and runs parallel to the main tectonic feature of the area under study, the Santorini – Amorgos Fault Zone (NE – SW direction). A strong anomaly shape smearing along cross section B (NE – SW direction) is observed, while no significant smearing occurs along cross section A (NW – SE direction) (Figure 6). This anomaly smearing occurs in a NE-SW direction, probably due to the fact that this cross section is parallel to the dominant direction of seismic rays. In particular, the majority of the earthquakes lies in the Coloumbo seamount area, while almost all the seismological stations are located on the Santorini complex. As a result, most seismic rays follow a mainly NE – SW direction, resulting in the observed NE – SW smearing. Moreover, it should be pointed out that this smearing is actually 3-D: rays emerging at depths of  $\sim 6 - 9$  km at the Coloumbo area are recorded at surface stations on Santorini, resulting in an NE – SW – upward smearing of velocity anomalies (Figure 6d). On the other hand, little smearing is observed in the perpendicular direction (NW – SE), suggesting that cross-sections with this orientation can provide more reliable information on the velocity structure.

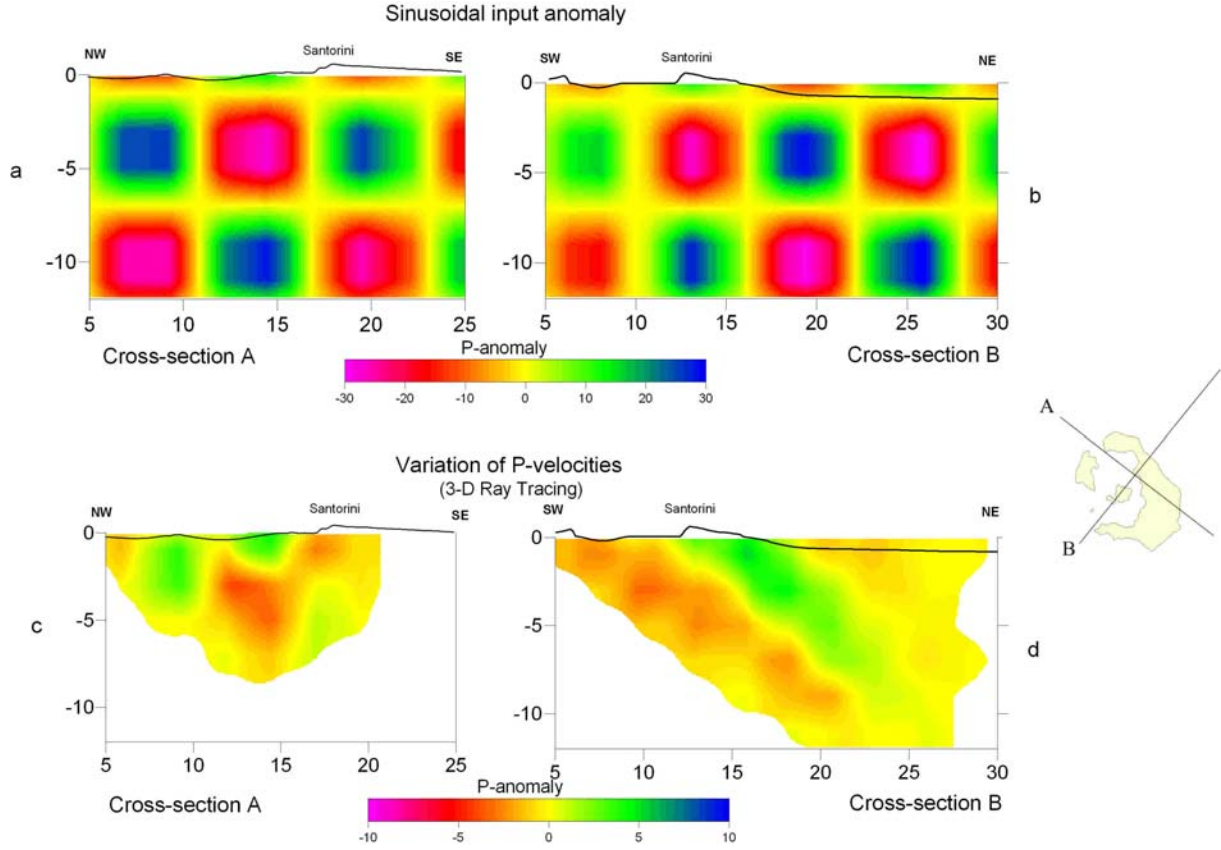


**Figure 6:** Variation of  $P$ -wave velocity along two cross-sections (A and B) (see small inset figure) of the input sinusoidal anomaly (a and b) and the inverted (c and d) velocity model. Notice the smearing along cross-section B, which is parallel to the dominant direction of seismic rays.

In order to summarize the results of the resolution tests, the average recovered anomaly amplitude is presented in Figure (7) as a function of the logarithm of the ray length (in km) associated with each velocity node. In general, for  $\log(\text{ray length}) > 1.6$  (associated ray length  $> \sim 40$  km) the recovered anomaly is of the order of  $\sim 20\%$  of the input anomaly. The ray length associated with each node appears to be a good index for the robustness of the inverted anomaly model, considering the observed anomaly shape smearing along the direction of the seismic rays and the resolution depth limit of 7 km. In all results later presented, no information is presented for nodes (cells) with a  $\log(\text{ray length})$  less than 1.6, hence an average  $\sim 20\%$  minimum anomaly recovery should be considered for the obtained results.

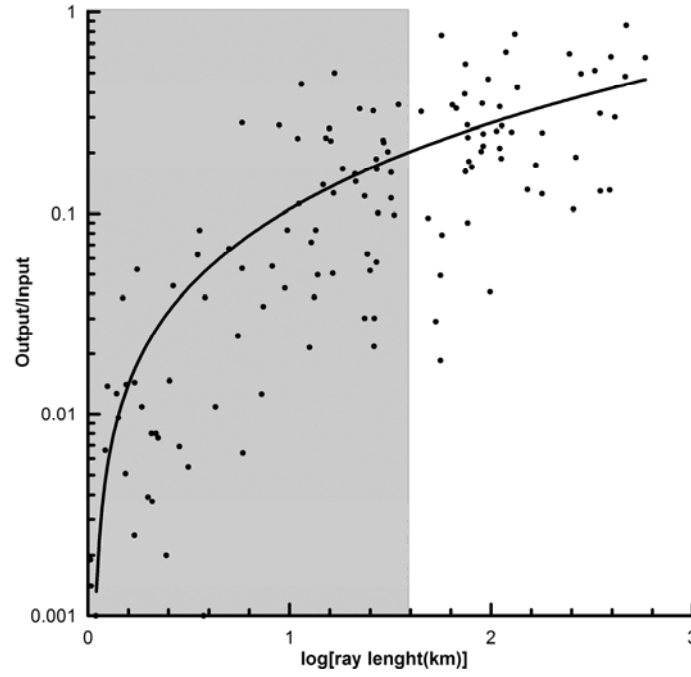


**Figure 7:** Variation of the amplitude of the recovered anomaly from the checkerboard pattern test, as a function of the logarithm of the ray length (in km) associated with each grid velocity node. No results were further considered for nodes with  $\log(\text{ray length}) < 1.6$ , corresponding to an average recovered anomaly of  $\sim 20\%$ .

## 6. Tomographic Results – Conclusions

In Figure (8), the histograms for the  $P$  and  $S$  residuals are plotted for the initial 1-D and final 3-D velocity models. The final residual distribution is clearly improved for both  $P$  and  $S$  arrivals. The standard deviations for the initial  $P$  and  $S$  residuals changed from 0.50 s and 0.60 s (1-D) to 0.25 s and 0.30 s (3-D), respectively. In both cases, the variance reduction is  $\sim 75\%$ , which confirms the impact of the three-dimensional velocity model.

The  $P$  and  $S$  velocity distributions derived from the final 3-d velocity model are shown in Figures (9) and (10), respectively. Very strong lateral velocity variations are recognized at all depths, especially at shallower depths (0 – 3 km). In particular, there is a low-velocity zone beneath the main caldera of the Santorini volcanic center with lower  $P$ -velocities ( $V_p \approx 5.0$  km/s) and  $S$ -velocities ( $V_s \approx 2.8$  km/s), in contrast with the high-velocity area in the SE part of main island of Santorini complex ( $V_p \approx 6.3$  km/s and  $V_s \approx 3.6$  km/s). This high velocity contrast corresponds to the difference between the low-velocity volcanic rocks of the intra-calderic area with the high-velocity bedrock formations of Mount Profitis Ilias located in the SE part of Santorini.

Moreover, there is a well-defined low-velocity zone, especially at depths between 5 and 7 km, which is crossing the cape Coloumbo at NE part of main Santorini Island following a NE-SW direction. This low-velocity zone is in very good agreement with the “Kameni-Coloumbo” fracture zone (NE-SW direction) in the same area, which has been observed from both neo-tectonic and seismological data (e.g. Mountrakis et al., 1996, Dimitriadis et al., 2009) (Figures 9 and 10).

Furthermore, several cross sections have been plotted in order to facilitate the overview and evaluation of the tomographic results. Four cross sections have been drawn parallel to a NW – SE direction (Figures 11a and 11b) and four additional ones were selected perpendicular to the first four sections, following a NE – SW direction (Figures 12a and 12b). In every cross section an exaggerated morphology profile is also plotted for a better overview.

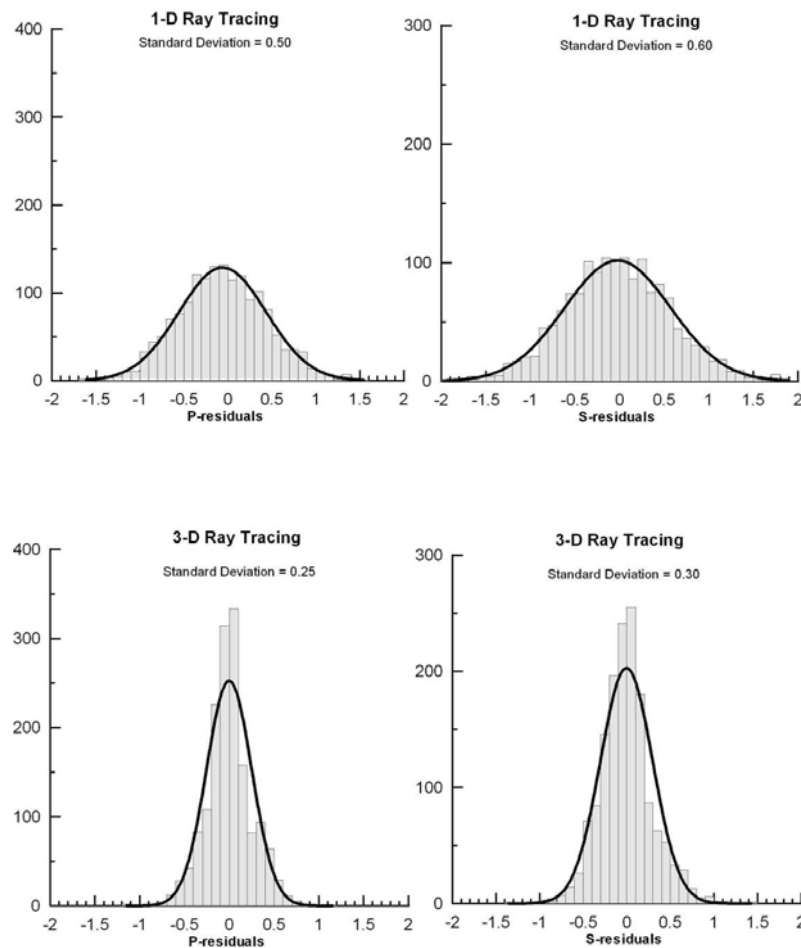


**Figure 8:** Histograms of the  $P$  and  $S$  residuals of the arrivals for the initial one-dimensional model (1-D) and the final three-dimensional model (3-D). A significant variance improvement is observed for the final 3-D model residual distribution for both  $P$  and  $S$  phases.

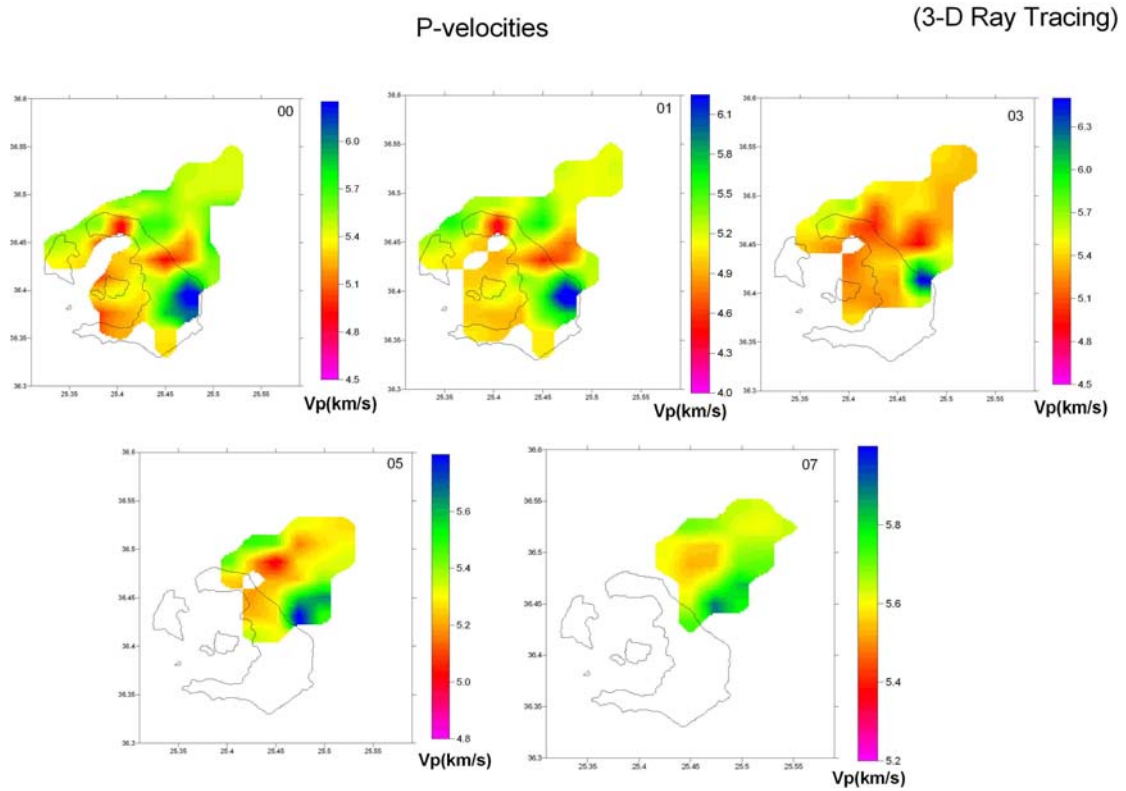


**Figure 9:** *P*-velocities derived from the final 3-d velocity model, up to the depth of 7 km, for the area under study. Strong lateral variations are recognized at all depths, reflecting the presence of low-velocity volcanic zones, in contrast with the high-velocity areas (SE Santorini) corresponding to the bedrock formations of the area under study.

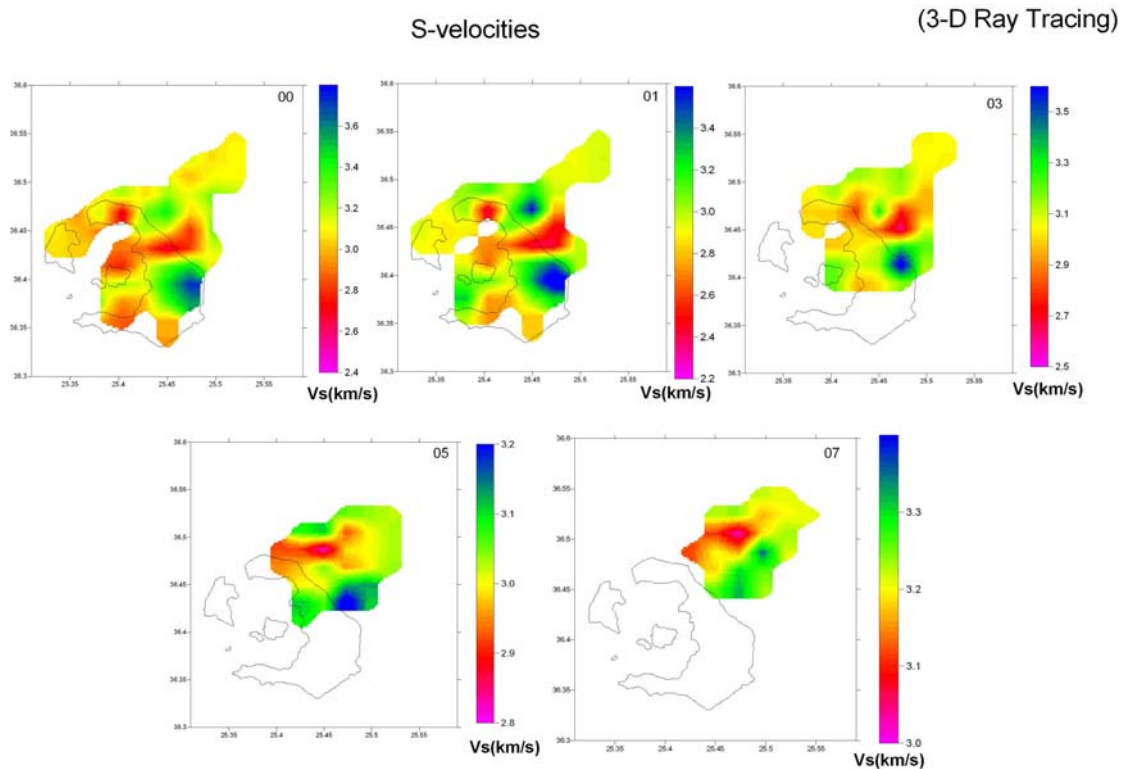


**Figure 10:** Same as Figure (9) for *S*-velocities.

In the first two cross sections (1 and 2 in Figures 11a and 11b) a strong velocity contrast is observed between the negative velocity anomalies of the main caldera of Santorini volcanic center and the high velocities of the southeastern part of the main Santorini Island (metamorphic bedrock of Mount Profitis Ilias). Furthermore, cross sections 2 and 3 (Figures 11a and 11b) depict clearly the low-velocity zone at the northeastern part of Santorini Island (NE – SW direction), which was also observed in the previous figures (Figures 9 and 10). In particular, this low-velocity zone seems to consist of two branches, both following the NW – SE direction; the first branch is located beneath Oia area (northern part of Santorini) and the second one is located beneath the northeastern coast of Santorini. As was previously mentioned, this zone is in good agreement with the “Kameni-Coloumbo” fracture zone, which is the western termination of the major tectonic feature of the broader area under study, the ENE – WSW Santorini – Amorgos Fault Zone. The low velocities observed suggest that this tectonic zone probably acts as a tecto-volcanic conduit connecting the Coloumbo volcanic seamount with the Santorini caldera (Figures 11a and 11b).

The magmatic chamber of Coloumbo volcanic center can be probably correlated with the negative velocity perturbation observed at the depth of 6-7 km (see cross-section 4 of Figure 11) in both P and S models. This assumption is in very good agreement with recent independent geophysical (Huebscher et al., 2006, Hensch et al., 2008), seismological (Bohnhoff et al., 2006) and geothermal (Sigurdsson et al., 2006) results for the same area.

Figures (12a) and (12b) presents four cross-sections with a NE – SW direction, parallel to the main tectonic feature of the Santorini – Coloumbo volcanic system, extending from the southern part of main Santorini Island to the Coloumbo volcanic center. The first two cross sections (cross sections 5 and 6) show a possible connection between the volcanic rocks of the caldera of Santorini volcanic center with the magmatic chamber beneath Coloumbo volcanic seamount. This low-velocity zone is following a NE – SW direction, parallel to the “Kameni-Coloumbo” fracture zone, suggesting the existence of a continuous volcanic area connecting the two volcanic centers, as previously mentioned (Figures 11 and 12). The last cross section (cross section 8 in Figures 12a and 12b) shows a strong positive velocity perturbation area, corresponding to the metamorphic rocks of the Profitis Ilias Mountain (southeastern part of the Santorini Island).

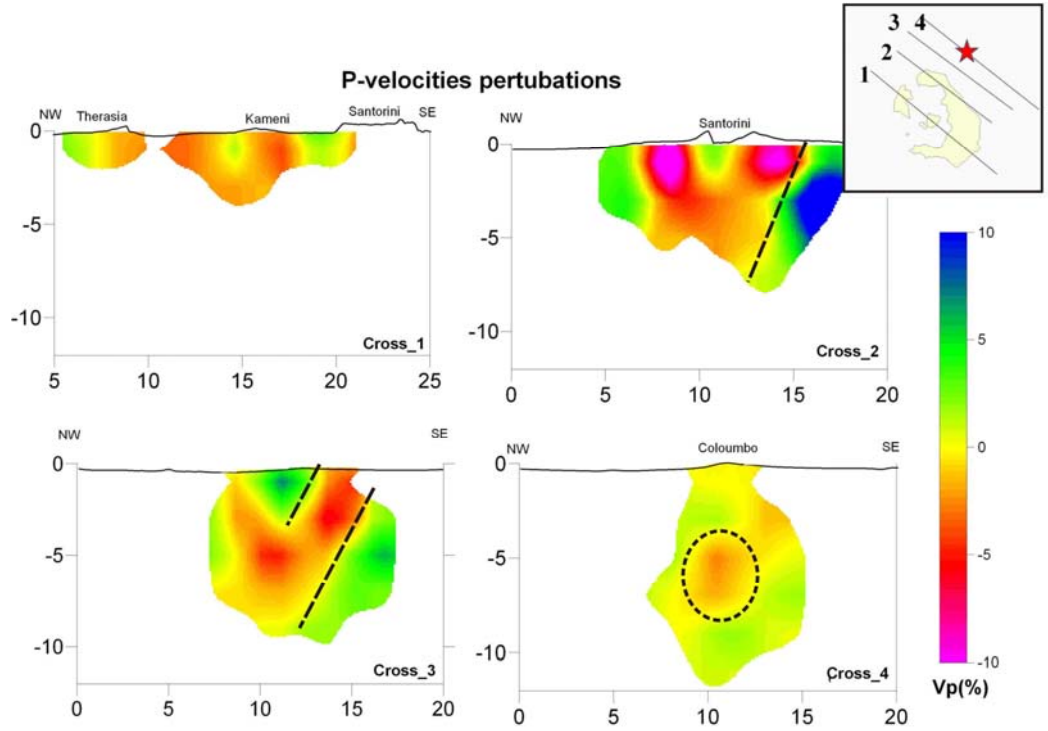


**Figure 11a:** P- velocity variation along four NW-SE trending cross-sections using the final 3-d velocity model. The position of the cross-sections and the Coloumbo seamount (red star) are shown in the embedded figure. A strong velocity contrast is observed between the volcanic rocks of the caldera and the bedrock formation (cross-section 2). Moreover, the “Kameni-Coloumbo” fracture zone (dashed lines) is identified in cross-sections 2 and 3 as a low velocity anomaly (see text for details), while the possible position of the Coloumbo low-velocity magmatic chamber is denoted with a dashed line in cross-section 4.

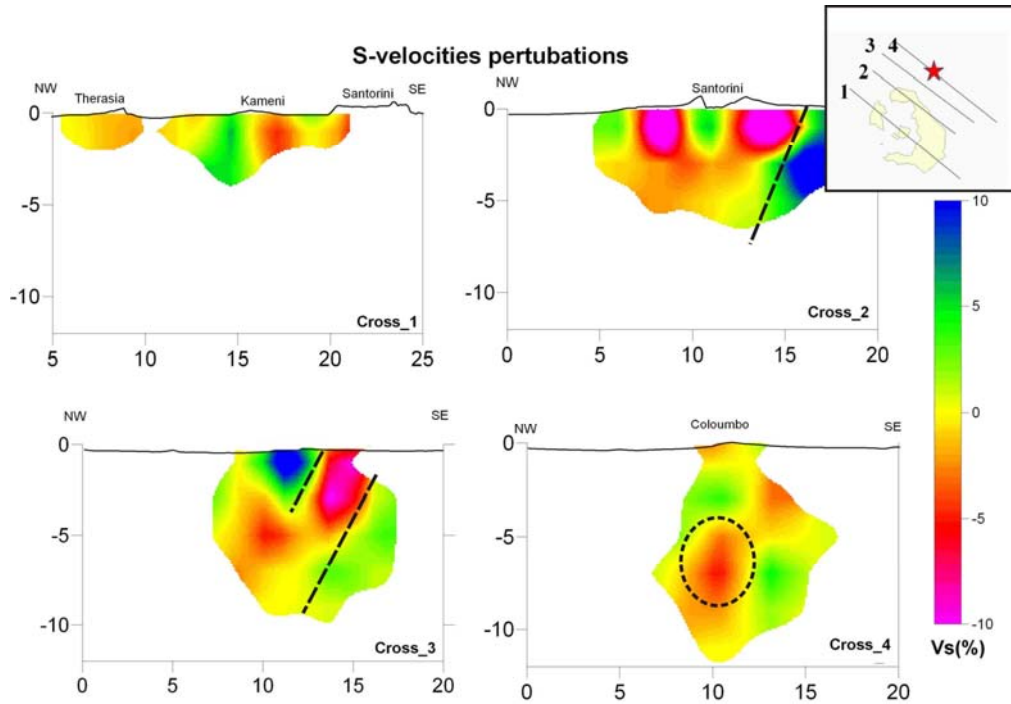


**Figure 11b:** Same as Figure (11a) for S-velocities.

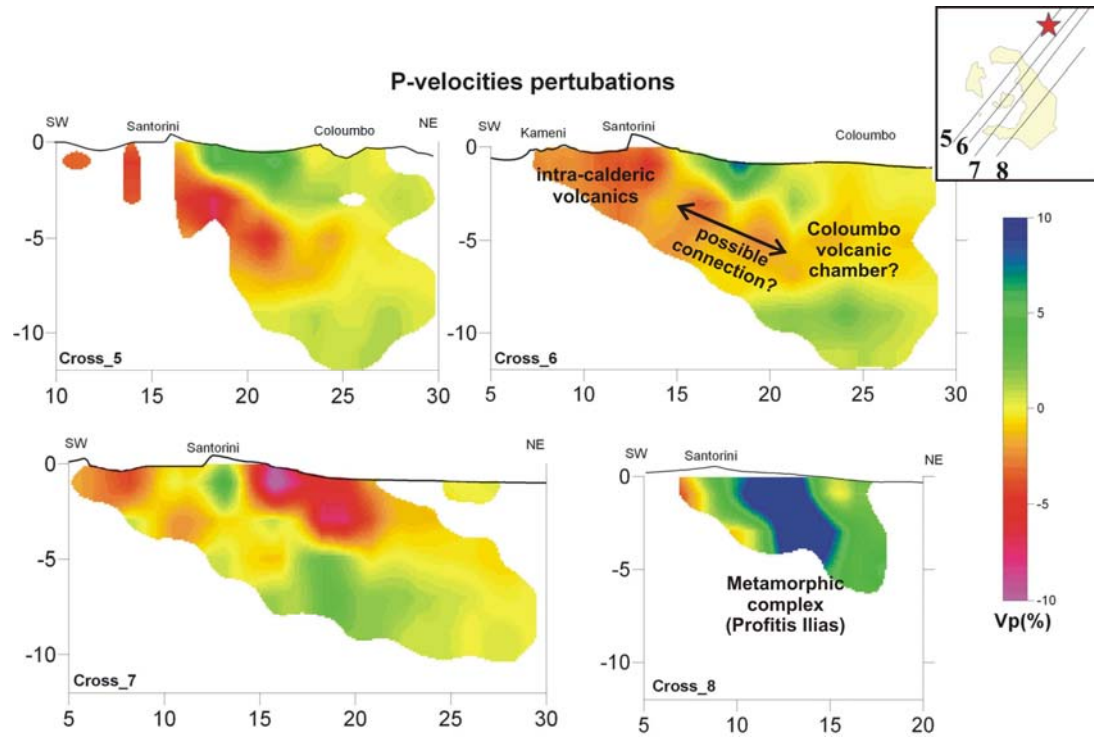


**Figure 12a:** Variation of *P*-wave velocity along four NE-SW cross-sections of the final 3-d velocity model. The position of the cross-sections and the Coloumbo seamount (red star) are shown in the embedded figure. Notice the possible connection between the magmatic material of Santorini and Coloumbo volcanic centers (cross-sections 5 and 6 see text for details) and the high-velocity province of the Profitis Ilias metamorphic bedrock (cross-section 4).

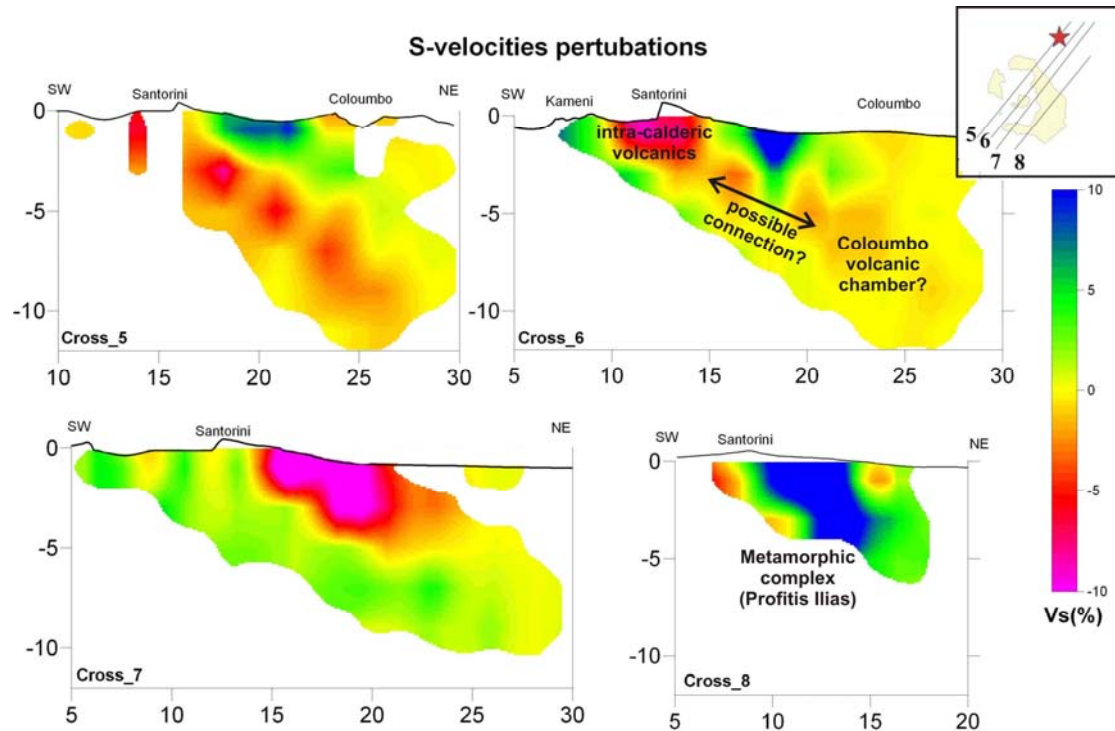


**Figure 12b:** Same as Figure (12a) for *S*-velocities.

The interpretation of the NE-SW cross-sections shown in Figures (12a) and (12b) should be considered with caution. As was demonstrated by the resolution tests (figure 6), an anomaly shape smearing is observed along NE – SW trending cross-sections, due to the preferential directivity of seismic rays. Therefore, although the position of the NW – SW anomalies is quite robust (see figure 6c), any conclusion about the continuity of the low-velocity zones observed along the NE – SW cross-sections is questionable. However, the individual low-velocity areas beneath the caldera of Santorini volcanic center and the Coloumbo seamount should be considered as reliable, since the corresponding anomalies are both identified in the NW – SE cross-sections, as well as in the horizontal depth sections.

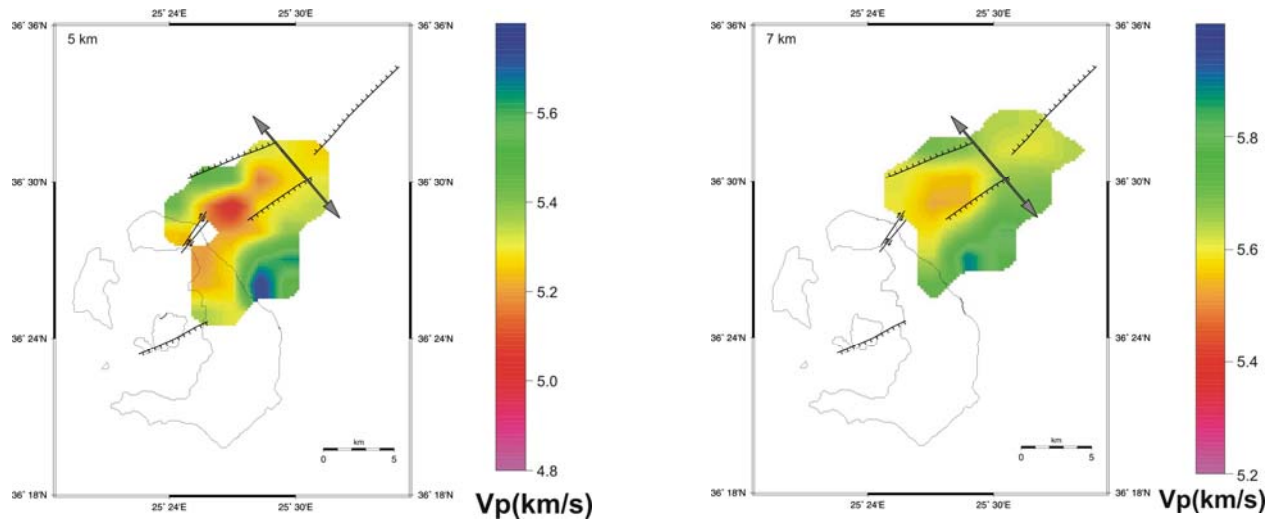


**Figure 13:** *P*-velocity distribution derived from the final 3-d velocity model for the depth of 5 km and 7 km of the study area. Main faults (Perissoratis, 1995; Mountrakis et al., 1996) are also depicted, along with the calculated stress orientation (small grey arrow) derived by Dimitriadis et al. (2009). Notice the excellent agreement of the neo-tectonic and seismic data regarding the Kameni-Coloumbo fracture zone with the presence of the shallow NE-SW trending low-velocity zone in the area under study (see text for details).

The Santorini – Coloumbo volcanic system is dominated by a NNW – SSE extensional stress regime that produces neotectonic lineaments, such as the “Kameni – Coloumbo” fracture zone (Fytikas et al., 1990; Vougioukalakis et al., 1994, 1995; Mountrakis et al., 1996; Francalanci et al., 2005; Vougioukalakis and Fytikas, 2005). This direction coincides with the alignment of the volcanic centers; hence it is reasonable to assume that this tectonic zone provides pathways for ascending volcanic

material (e.g. dykes). This pattern can be correlated with the NE-SW low-velocity lineament observed at the northeastern part of Santorini Island, especially at depths between 5 and 7 km, in very good agreement with the tectonic regime of the broader area under study (Figure 13). In particular, the low velocities are in good agreement with the observed faults in the examined area, with a direction similar to the dominant “Kameni-Coloumbo” fracture zone, perpendicular to the extensional stress field determined for this area from recent studies (e.g., Dimitriadis et al., 2009). The observed low-velocity zone is also in very good agreement with neo-tectonic observations at the northeastern part of Santorini Island (Cape Coloumbo area) where oblique strike-slip faults have been observed (Mountrakis et al., 1996) (Figure 13).

## **7. Acknowledgements**

This work was partially funded by the PYTHAGORAS research program of the Hellenic Ministry of Education (Research Committee of University of Thessaloniki #21945#).

## References

- Aki, K. and Lee, W. H. K., 1976. Determination of three-dimensional velocity anomalies under a seismic array using first P arrival times from local earthquakes: A homogeneous initial model. *Journal of Geophysical Research* 81, pp. 4381-4399.
- Bohnhoff, M., Rische, M., Meier, T., Endrun, B., Harjes, H.-P., and Stavrakakis, G., 2004. A temporary seismic network on the Cyclades (Aegean Sea, Greece). *Seismol. Res. Letters* 75/3, pp. 352–357.
- Bohnhoff, M., Rische, M., Meier, T., Becker, D., Stavrakakis G., and Harjes, H.-P., 2006. Micro seismic activity in the Hellenic Volcanic Arc, Greece, with emphasis on the seismotectonic setting of the Santorini-Amorgos zone. *Tectonophysics* 423, Issues 1-4, pp. 17-33.
- Crosson, R. S., 1976. Crustal Structure Modeling of Earthquake Data: Simultaneous Least Squares Estimation of Hypocenter and Velocity Parameters. *Journal of Geophysical Research* 81, pp. 3036-3046.
- Dimitriadis I. M., Panagiotopoulos D. G., Papazachos C. B., Hatzidimitriou P. M., Karagianni E. E. and Kane I., 2005. Recent seismic activity (1994-2002) of the Santorini volcano using data from local seismological network. *The South Aegean Active Volcanic Arc: Present Knowledge and Future Perspectives (Developments in Volcanology, Volume 7)*, pp. 185-203.
- Dimitriadis I., Karagianni E., Panagiotopoulos D., Papazachos C., Hatzidimitriou P., Bohnhoff M., Rische M. and T. Meier, 2009. Seismicity and active tectonics at Coloumbo Reef (Aegean Sea, Greece): Monitoring an active volcano at Santorini Volcanic Center using a temporary seismic network. *Tectonophysics* 465, pp. 136-149.
- Francalanci, L., Vougioukalakis, G., Perini, G. and Manetti, P., 2005. A West-East Traverse along the magmatism of the south Aegean volcanic arc in the light of volcanological, chemical and isotope data. *The South Aegean Active Volcanic Arc: Present Knowledge and Future Perspectives (Developments in Volcanology, Volume 7)*, pp. 65-111.
- Franklin, J. N., 1970. Well-posed stochastic extension of ill-posed linear problems. *J. Math. Anal. Appl.*, 31, pp. 682-716.

- Fytikas, M., Kolios, N. and Vougioukalakis, G., 1990. Post-Minoan Volcanic Activity of the Santorini Volcano: Volcanic hazard and risk, forecasting possibilities. *In: Hardy, D.A., (Editor), Thera and the Aegean World III, 2.* The Thera Foundation, London, pp. 183-198.
- Hensch, M., Dahm, T., Hort, M., Dehghani, A., Hübscher, C., and the EGELADOS working group, 2008. First results of the Ocean-Bottom-Seismometer and-Tiltmeter experiment at Coloumbo submarine volcano (Aegean Sea, Greece), *Geophysical Research Abstracts, Vol. 10, EGU2008-A-02760*, EGU General Assembly 2008.
- Huebscher, C., Hensch, M., Dahm, T., Dehgani, A., Dimitriadis, I., Hort, M., and T., Taymaz, 2006. Toward a Risk Assessment of Central Aegean Volcanoes. *EOS, Vol. 87, No. 39, 26 September 2006*, pp. 401-407.
- Humphreys, E., and R. W. Clayton, 1988. Adaptation of back projection tomography to seismic travel time problems. *J. Geophys. Res.*, 93, pp. 1073-1085.
- Kissling, E., Ellsworth, W. L., Eberhart-Phillips, D. and Kradofler, U., 1994. Initial reference model in local earthquake tomography. *J. Geophys. Res.*, 99, pp. 19635-19646.
- Kissling, E., Husen, S., and Haslinger, F., 2001. Model parametrization in seismic tomography: a choice of consequence for the solution quality. *Physics of The Earth and Planetary Interiors, Volume 123*, pp. 89-101.
- McClusky, S. Balasdsanian, A. Barka, C. Demir, I. Georgiev, M. Hamburger, K. Hurst, K. Kastens, G. Kekelidze, R. K. V. Kotzev, O. Lenk, S. Mahmoud, A. Mishin, M. Nadariya, A. Ouzounis, D. Paradissis, Y. Peter, M. Prilepin, R. Reilinger, I. Sanli, H. Seeger, A. Tealeb, M. N. Toksoz and G. Veis, 2000. Global positioning system constraints on crustal movements and deformations in the eastern Mediterranean and Caucasus. *Journal of Geophysical Research* 105, pp. 5695–5719.
- McKenzie, D. P, 1972. Active tectonics of the Mediterranean region. *Geophysical. J. R. astr. Soc.*, 30, pp. 109-185.
- Meier, T., Rische, M., Endrun, B., Vafidis, A. and Harjes, H. -P., 2004, Seismicity of the Hellenic subduction zone in the area of western and central Crete observed by temporary local seismic networks, *Tectonophysics*, 383, pp. 149-169
- Moser, T. J., 1991. Shortest path calculation of seismic rays. *Geophysics*, 56, pp. 59-67.

- Moser, T. J., G. Nolet, and R. Snieder, 1992. Ray bending revisited. *Bull. Seismol. Soc. Am.*, 82, pp. 259-289.
- Mountrakis, D. M., Pavlides, S. B., Chatzipetros, A., Meletlidis, S., Tranos, M. D., Vougioukalakis, G. and Kiliass, A. A., 1996. Active deformation of Santorini. *Proceedings of 2nd Workshop on European Laboratory Volcanoes, May 2-4 1996, Santorini, Greece*, pp. 13-22.
- Paige, C. C., and Saunders, M. A., 1982. LSQR: Sparse linear equations and least squares problems, *ACM Transactions on Mathematical Software* 8/2, pp. 195–209.
- Papazachos, B. C. and Comninakis, P. E., 1971. Geophysical and tectonic features of the Aegean arc. *Journal of Geophysical Research* 76, pp. 8517-8533.
- Papazachos, B. C., Karakostas, B. G., Papazachos C. B., and Scordilis, E. M., 2000. The geometry of the Wadati – Benioff zone and lithospheric kinematics in the Hellenic arc. *Tectonophysics* 319, pp. 275-300.
- Papazachos, B. C., Dimitriadis, S. T., Panagiotopoulos, D. G., Papazachos, C. B. and Papadimitriou, E. E., 2005. Deep structure and active tectonics of the southern Aegean volcanic arc. *The South Aegean Active Volcanic Arc: Present Knowledge and Future Perspectives (Developments in Volcanology, Volume 7)*, pp. 47-64.
- Papazachos, C. B. and Nolet, G., 1997a. *P* and *S* deep structure of the Hellenic area obtained by robust non-linear inversion of travel times. *Journal of Geophysical Research* 102, pp. 8349-8367.
- Papazachos, C. B. and Nolet, G., 1997b. Non-linear arrival time tomography. *Annali di Geofisica Vol. XL, (1)*, pp. 85-97.
- Perissoratis, C., 1995. The Santorini volcanic complex and its relation to the stratigraphy and structure of the Aegean arc, Greece. *Marine Geology*, 128, pp. 37-58.
- Sambridge, M. S., 1990. Non-linear arrival time inversion: Constraining velocity anomalies by seeking smooth models in 3-D. *Geophys. J. Int.*, 101, pp. 157-168.
- Sigurdsson, H., Carey, S., Alexandri, M., Vougioukalakis, G., Croff, K., Roman, C., Sakellariou, D., Anagnostou, C., Rousakis, G., Ioakim, C., Gogou, A., Ballas, D., Misaridis, T., and P., Nomikou, 2006. Marine Investigations of Greece's Santorini Volcanic Field. *EOS, Vol. 87, No. 34, 22 August 2006*, pp. 337-348.

- Spakman, W., 1988. Upper mantle delay-time tomography with an application to the collision zone of the Eurasian, African and Arabian plates. *Ph.D. Thesis, Utrecht University, the Netherlands*.
- Tarantola, A., 1987. Inverse Problem Theory. Elsevier B. V., Netherlands (pp. 613).
- Thurber, C. H., 1983. Earthquake Locations and Three-Dimensional Crustal Structure in the Coyote Lake Area, Central California. *Journal of Geophysical Research* 88, pp. 8226-8236.
- Vougioukalakis, G., Mitropoulos, D., Perissoratis, C., Andrinopoulos, A., and Fytikas, M., 1994. The submarine volcanic centre of Coloumbo, Santorini, Greece. *Bulletin of Geological Society of Greece*, XXX/3, pp. 351-360.
- Vougioukalakis, G., Francalanchi, L. Serana, A. and Mitropoulos, D., 1995. The 1649-1650 Coloumbo submarine volcano activity, Santorini, Greece. In: Barberi, F., Casale, R., and Fratta, M., (editors), "The European Laboratory Volcanoes, Workshop Proceedings", European Commission, European Science Foundation, Luxemburg, pp. 189-192.
- Vougioukalakis, G. E., and Fytikas, M., 2005. Volcanic hazards in the Aegean area, relative risk evaluation, monitoring and present state of the active volcanic centers, *The South Aegean Active Volcanic Arc: Present Knowledge and Future Perspectives (Developments in Volcanology, Volume 7)*, pp. 161–183.
- Waldhauser, F. and Ellsworth, W. L., 2000. A double-difference earthquake location algorithm: Method and application to the northern Hayward Fault, California. *Bull. Seismol. Soc. Am.*, 90, pp 1353–1368.
- Waldhauser, F., 2001. HypoDD: A computer program to compute double-difference hypocenter locations, U.S. Geological Survey Open File Report, 01-113, pp. 25.
- Wielandt, E., 1987. On the validity of the ray approximation for interpreting delay times. In: Nolet, G., (editor), "Seismic Tomography", Reidel, Norwell, Mass., pp. 85-98.